

## MIT Open Access Articles

*Back-to-Basics tutorial: X-ray diffraction of thin films*

The MIT Faculty has made this article openly available. **Please share** how this access benefits you. Your story matters.

**Citation:** Harrington, George F. and Santiso, José. 2021. "Back-to-Basics tutorial: X-ray diffraction of thin films."

**As Published:** <https://doi.org/10.1007/s10832-021-00263-6>

**Publisher:** Springer US

**Persistent URL:** <https://hdl.handle.net/1721.1/143483>

**Version:** Author's final manuscript: final author's manuscript post peer review, without publisher's formatting or copy editing

**Terms of Use:** Article is made available in accordance with the publisher's policy and may be subject to US copyright law. Please refer to the publisher's site for terms of use.



## Back-to-Basics tutorial: X-ray diffraction of thin films

**Cite this Accepted Manuscript (AM) as:** Accepted Manuscript (AM) version of George F. Harrington, José Santiso, Back-to-Basics tutorial: X-ray diffraction of thin films, Journal of Electroceramics <https://doi.org/10.1007/s10832-021-00263-6>

This AM is a PDF file of the manuscript accepted for publication after peer review, when applicable, but does not reflect post-acceptance improvements, or any corrections. Use of this AM is subject to the publisher's embargo period and AM terms of use. Under no circumstances may this AM be shared or distributed under a Creative Commons or other form of open access license, nor may it be reformatted or enhanced, whether by the Author or third parties. See here for Springer Nature's terms of use for AM versions of subscription articles: <https://www.springernature.com/gp/open-research/policies/accepted-manuscript-terms>

The Version of Record of this article, as published and maintained by the publisher, is available online at: <https://doi.org/10.1007/s10832-021-00263-6>. The Version of Record is the version of the article after copy-editing and typesetting, and connected to open research data, open protocols, and open code where available. Any supplementary information can be found on the journal website, connected to the Version of Record.

# Back-to-Basics Tutorial: X-ray diffraction of thin films

George F. Harrington<sup>\*a,b,c,d</sup>, José Santiso<sup>e</sup>

<sup>a</sup>Center of Coevolutionary Research for Sustainable Communities (C<sup>2</sup>RSC), Kyushu University, 744 Motooka, Nishi-ku, Fukuoka 819-0395, Japan

<sup>b</sup>Next-Generation Fuel Cell Research Centre, Kyushu University, 744 Motooka, Nishi-ku, Fukuoka 819-0395, Japan

<sup>c</sup>Department of Materials Science and Engineering, Massachusetts Institute of Technology, 77 Massachusetts Ave., Cambridge MA 02139, U.S.A.

<sup>d</sup>International Institute for Carbon-Neutral Energy Research (I<sup>2</sup>CNER), Kyushu University, 744 Motooka, Nishi-ku, Fukuoka 819-0395, Japan

<sup>e</sup>Catalan Institute of Nanoscience and Nanotechnology (ICN2), CSIC and Barcelona Institute of Science and Technology (BIST), Campus UAB, Bellaterra, Barcelona, 08193, Spain

\*Corresponding Email: harrington.frederick.george.302@m.kyushu-u.ac.jp

## Abstract

X-ray diffraction (XRD) is an indispensable tool for characterising thin films of electroceramic materials. For the beginner, however, it can be a daunting technique at first due to the number of operation modes and measurements types, as well as the interpretation of the resultant patterns and scans. In this tutorial article, we provide a foundation for the thin-film engineer/scientist conducting their first measurements using XRD. We give a brief introduction of the principle of diffraction and description of the instrument, detailing the relevant operation modes. Next, we introduce five types of measurements essential for thin film characterisation:  $2\theta/\omega$  scans, grazing-incidence scans, rocking curves, pole figures, and azimuth scans (or  $\phi$  scans). Practical guidelines for selecting the appropriate optics, mounting and aligning the sample, and selecting scan conditions are given. Finally, we discuss some of the basics of data analysis, and give recommendations on the presentation of data. The aim of this article is to ultimately lower the barrier for researchers to perform meaningful XRD analysis, and, building on this foundation, find the existing literature more accessible, enabling more advanced XRD investigations.

## Introduction

Thin films are excellent model systems to study electroceramic materials. Possessing a well-defined

**Part of the Back-to-Basics Tutorial Series:**

In this **Back-to-Basics** article series, we aim to lower the entrance barrier for researchers carrying out measurements in a given technique for the first time by establishing a series of tutorials, each on a specific experimental technique or method applied to electroceramic materials. Each article will impart a basic understanding and provide practical guidelines for the beginner. Through the **Back-to-Basics** series, we hope to collectively gather the community's experience on experimental research in a way that will ultimately serve the needs of as broad an audience as possible.

geometry and a microstructure that can be tailored via fabrication or post-treatment conditions, thin films represent an indispensable approach to investigate interfacial, microstructural, or confinement effects in oxides. More complex thin film structures can also be engineered, such as multilayers, nanocomposite films, layers with a graded composition, and ultimately superlattices. Direct technological applications of oxide films also exist in microelectronics, optics, optoelectronics, information storage, photovoltaics, miniaturised electrochemical energy storage and conversion devices, and protective coatings in metallurgy and bio-implants.

Dramatic differences in physical and chemical properties can exist between thin films and their bulk ceramic counterparts. These include, but are not limited to: (1) geometric differences such as thickness and surface roughness that also leads to a much higher surface/interface volume fraction, (2) grain sizes from <10 nm in polycrystalline films to epitaxial films which behave as a single crystal, (3) preferential orientations and texture ranging from randomly oriented grains to monoaxial (fiber) texture to biaxial texture, (4) differences in crystallinity, (5) strains/stresses occurring in the film, and (6) compositional differences from bulk materials or even compositional gradients. These differences between bulk and thin film materials are often directly related to the growth conditions under which the films have been fabricated and can have substantial impact on the functional properties. Hence there is a *growth-structure-function* relationship within film engineering, such that understanding the structure is vital to tailor the growth conditions and engineer the functional properties. Further, reproducibility is often an issue in physical vapour deposition (PVD) or chemical vapour deposition (CVP) methods, and therefore tools to routinely characterise thin films are of the upmost importance to the thin film engineer/scientist. Fortunately, X-ray diffraction (XRD) provides such a tool, and is *arguably* the most useful and versatile technique in the characterisation of thin films.<sup>1</sup> XRD can be used to obtain the following information on thin films:

- Crystalline phase and lattice parameters
- Degree of crystallinity
- Degree and nature of preferential orientation or texture of the crystalline grains
- Grain size
- Density of dislocations

<sup>1</sup> The case for transmission electron microscopy (TEM) as a comparatively useful tool could certainly be made but should be seen as a complementary technique for spatially resolved characterisation within films.

- Residual stress/strain in the film
- Film composition (via the lattice parameters)
- Film thickness

The advantages and disadvantages of XRD as a technique to investigate thin films are given in Box 1.

The purpose of this article is to give an introduction to researchers making their first measurements on thin films using XRD. Rather than focusing on formally introducing the theory behind XRD, here we aim only to provide the basic information needed and instead focus on providing guidelines on the procedures for setting up, performing, and interpreting routine XRD measurements on thin films. This is by no means a comprehensive article, and we have made the (difficult) decision to restrict the guidelines to five basic measurements: Symmetric  $2\theta/\omega$  scans, grazing-incidence scans, rocking curves,  $\phi$ -scans, and pole figures. The interested reader is strongly encouraged to explore the further reading and online resources referenced at the end of the article.

Throughout this article we will assume the reader has a basic understanding of crystal structure and the relevant notation, as well as of microstructure of ceramic materials. We also must remind the reader that X-rays are extremely hazardous, and although safety features on modern diffractometers make the risk of exposure almost negligible, one must ensure that they abide by the safety regulations of the institute and laboratory. Please always consult the manager of the XRD facility before carrying out any measurements.

#### **Box 1**

##### **Advantages:**

- → Relatively fast.
- → Non-destructive.
- → Very precise, and, if done correctly, accurate.
- → Probes a large proportion of the area of the film.
- → Measurements under non-ambient conditions and *in-situ* measurements possible.

¶

##### **Disadvantages:**

- → Spatial resolution is poor, and often non-existent<sup>2</sup>
- → Some information can be hard to deconvolute, for example, compositional changes and strain in films will both lead to shifts in peak positions.

## Underlying theory

There are two underlying principles that give rise to diffraction of X-rays from crystalline materials. The first is that elastic (Thomson) scattering of photons allows us to invoke the laws of specular reflectance and treat atomic planes as mirrors.<sup>3</sup> The second is that the wavelength of X-rays is of the same order of magnitude as the interatomic distances in crystals (0.15 – 0.5 nm) which leads to constructive and destructive interference phenomena.

The diffraction of X-rays is best visualised as shown in **Fig. 1**, where an X-ray beam, of wavelength  $\lambda$ , is incident at an angle,  $\theta$ , onto a series of atomic planes of spacing,  $d$ . The X-ray beam scatters off the planes at an angle,  $\theta$ , equal to the incident angle with respect to the crystalline plane. The relative phase shifts between X-rays scattered off the first and second planes, is given by the distance marked in orange in **Fig. 1**. From geometric considerations, it is therefore simple to show that constructive interference will take place for certain angles,  $\theta_B$ , depending on the interplanar spacing,  $d$ , according to

$$n\lambda = 2d_{hkl}\sin\theta_B \quad (1)$$

Eq. 1 is known as the Bragg Equation,  $\theta_B$  is referred to as the Bragg angle, and the  $hkl$  subscript of the interplanar spacing,  $d$ , refers to the Miller indices of the crystallographic plane.  $n$  is an integer and is referred to as the order of the diffraction maxima, with  $n = 1$  being the first order, and  $n = 2$  being the second order, and so on. The Bragg Equation relates the angular position of diffracted X-rays to the lattice spacing and underpins all XRD measurements.

**Fig. 1** Visualisation of Bragg's Equation

## The instrument

An X-ray diffractometer consists of five major components: The X-ray source, the detector, the incident (or primary beam) optics, the receiving (or diffracted beam) optics, and the goniometer, as shown in **Fig. 2**. The diffractometer is contained within a radiation enclosure and controlled by a computer. In this section, we give a brief outline of the major components and detail some of the different possible configurations for thin film measurements.

**Fig. 2** Components of a diffractometer

<sup>2</sup> Although it is possible to probe different sample depths, an exact quantification is difficult. A lab-based diffractometer typically analyses an area of a few mm<sup>2</sup> to cm<sup>2</sup>. Micro-XRD ( $\mu$ XRD) mapping with a small probing beam is possible but not particularly high resolution in lab-based diffractometers ( $\sim 100$ s  $\mu$ m), however some synchrotron-based facilities can achieve spatial resolutions of  $\sim 100$  nm.

<sup>3</sup> Obviously, this is not strictly true, but is a useful working assumption.

### The source

In a laboratory diffractometer, X-rays are produced in an evacuated X-ray tube, where electrons are produced by thermionic emission from a heated tungsten cathode, accelerated to a high energy, and collide with an anode target made from a specific high-purity metal. The electron current between the cathode and anode is adjustable and typically in the range of 10s to 100s of mA. The accelerating voltage is also variable and must be high enough (10s of kV) that when electrons impact the anode they cause atoms in the target to undergo ionization and subsequent electronic relaxation and emission of radiation. The resultant radiation has a characteristic wavelength dependent on the target material and the energy levels of the excited and relaxing electrons. A schematic of typical X-ray emission spectra is shown in **Fig. 3a**.

In regular diffraction work, the strongest characteristic radiation comes from the K set of which the most intense lines are the  $K_{\alpha 1}$ ,  $K_{\alpha 2}$ , and  $K_{\beta}$ .<sup>4</sup> By far the most common anode material is Cu,<sup>5</sup> and the wavelengths for the characteristic radiation are given in **Table 1**. The wavelength of  $K_{\alpha 1}$  and  $K_{\alpha 2}$  are very close and sometimes cannot be resolved. When they can be resolved they are referred to as the  $K_{\alpha}$  *doublet*; when they cannot be resolved are then denoted as the  $K_{\alpha}$  *line*, and the wavelength is taken as a weighted average of the  $K_{\alpha 1}$  and  $K_{\alpha 2}$  wavelengths.  $K_{\beta}$  radiation is undesirable when performing XRD and is usually removed using either a Ni filter<sup>6</sup> or a monochromator in the X-ray path (see Box 2). The other wavelength that the one should be aware of is tungsten contamination on the anode target originating from the cathode, which may cause additional peaks in the diffractogram, especially from very high intensity substrate peaks.<sup>7</sup>

**Table 1** Wavelengths of characteristic radiation from an X-ray tube with a Cu target [1]

| Characteristic radiation | $\lambda$ (Å) |
|--------------------------|---------------|
| Cu $K_{\alpha 1}$        | 1.54059       |
| Cu $K_{\alpha 2}$        | 1.54443       |
| Cu $K_{\alpha}$          | 1.5418        |
| Cu $K_{\beta}$           | 1.39223       |
| W $L_{\alpha 1}$         | 1.4764        |

<sup>4</sup> This is Siegbahn notation which describes the electron shell that loses an electron during ionisation, with K ( $n = 1$ , where  $n$  is the principal quantum number) being the innermost shell. Relaxation of an electron into the K shell from the second innermost shell (L,  $n = 2$ ) is denoted by an  $\alpha$  subscript, and from the third innermost shell (M,  $n = 3$ ) by a  $\beta$  subscript. The 1 and 2 subscripts denote the slight energy differences from electrons in the shell due to interactions between the spin and orbital momentum.

<sup>5</sup> Different materials such as Cr, Fe, Co, Ni, Mo, or Ag can also be used if the wavelength is more suitable for investigating a particular range of d-spacings. Cu  $K_{\alpha}$  radiation will cause materials containing Fe and Co to fluoresce as they are irradiated, making use of a different anode material sometimes necessary.

<sup>6</sup> Different metal filters are used depending on the choice of anode material.

<sup>7</sup> The intensity of the peaks originating from W contamination will depend on the age of the X-ray tube.

A schematic of an X-ray tube is given in **Fig. 3b**. Electrons from the cathode are focused onto the anode as a strip, and the generated X-rays pass through one of several beryllium windows. Depending on the window used, the X-rays emerge either as a line or a spot. This is referred to as *line focus* or *point focus*, respectively, and generally can be selected by rotating the tube in the diffractometer by 90° to align a different window with the incident optics. As discussed below, certain measurements are best performed under either line or point focus conditions.

The anode needs to be continuously water-cooled to prevent it from melting due to the heat introduced by the impinging electron current. Rotating anode designs exist that dissipate the heat over the anode target more effectively, which allows a greater current of electrons to be used resulting in a higher X-ray flux. Cathode filaments have a limited lifetime and should not be kept on for long periods of time if not used.<sup>8</sup> Turning on and shutting down, however, also degrades the filament and therefore should be done by slowly increasing the current and voltage and only carried out when necessary. XRD can also be carried out at synchrotron facilities, which can produce high intensity, highly monochromatic, and spatially well-defined X-rays.

One of the most important devices in an X-ray diffractometer is the safety shutter on the X-ray tube. This allows work such as changing optical components, inserting filters or attenuators, or changing samples to be safely carried out within the diffractometer enclosure while the X-ray tube is operating. It is of the utmost importance that the XRD user be aware of the status of the shutter through the various indicators of the instrument when carrying out measurements.

**Fig. 3** (a) Schematic of emission profiles emitted from an anode for several accelerating voltages. (b) Schematic of an X-ray tube with line focus and point focus windows

### *The detector*

In the diffractometer, the detector is used to convert the incoming X-rays to an electrical signal. The unit used is usually counts per second (cps). Detectors are often defined by their dimensionality, and can be point detectors (0D), line detectors (1D), or area detectors (2D). Working principles can also vary between different detectors, and common types include proportional counters, scintillation counters, and solid-state detectors. Although we won't go into the working details of each type here, the XRD user should be aware of the type of detector, and, crucially, the maximum count rate that the detector can reliably and safely measure (usually 10<sup>5</sup>-10<sup>6</sup> cps or 10<sup>4</sup> for solid-state detectors). A high intensity of X-rays can lead to a non-linear response or even damage the detector, and so attenuators (see Section 3.4) should be used for strongly diffracting peaks, such as those originating from single-crystal substrates or highly oriented films, as well as aligning the optical components where the beam travels directly from the source to the detector. Another important point to note, is that newer solid-state detectors (0D, 1D, and 2D) can discriminate a narrow energy window avoiding the

<sup>8</sup> X-ray tubes also require substantial amounts of electrical power to operate.



need for filters or monochromators (see Box 2) to reduce fluorescence, white radiation or even the  $K_{\beta}$  component.

### *The goniometer*

The angles between the source, detector, and sample surface are set by the goniometer. At its most basic, a diffractometer must be able to vary the angle between the source and the sample surface,  $\theta$ , and the angle between the incident beam and the detector,  $2\theta$ . Often diffractometers only have these two degrees of freedom, and are referred to as powder diffractometers, due to the vast numbers of powder samples measured on them. In powder diffraction, the incident and diffracted beam angles are coupled, and always moved simultaneously during a measurement such that  $2\theta$  is always exactly twice  $\theta$ . For thin film measurements, it is often necessary to decouple the scattering angle from the angle of incidence, such as in rocking curve measurements or when aligning the substrate, so  $\omega$  is used to denote the incident angle.

In some diffractometers the sample is fixed, either horizontally or vertically, and the tube and detector rotate in opposite directions, known as  $\Theta$ - $\Theta$  goniometers. Another diffractometer design is to keep the X-ray tube fixed, rotate the vertically mounted sample ( $\omega$  angle), and rotate the detector at twice the speed, referred to as  $\Theta/2\Theta$  goniometers. In most cases sample stages can move in the z direction and sometimes may also move laterally in the x and y directions, as depicted in **Fig. 4**.

Additional degrees of freedom are necessary for determining in-plane texture, via pole figures, which are the tilting angle,  $\psi$ , and the rotation or azimuth angle,  $\phi$ . The angles are shown schematically in **Fig. 4**. Often  $\chi$  is also used to denote the tilting angle, which is related to  $\psi$  according to  $\chi = 90^\circ - \psi$ . These added degrees of freedom are made possible by the use of a *Euler cradle*, which is an additional goniometer positioned within the  $2\theta/\omega$  circle. Such an instrument is often referred to as a *four-axis* or *four-circle* diffractometer, due to the four degrees of freedom  $\omega$ ,  $2\theta$ ,  $\psi$  and  $\phi$ . *Five-axis* and *six-axis* diffractometers also exist, which have further degrees of freedom for less conventional diffraction measurements, but a description of these are beyond the scope of this article.

**Fig. 4** Schematic of the notation used for the angles and degrees of freedom in a typical diffractometer used for thin film measurements

### *Incident and receiving optics*

Depending on the type of measurement, an appropriate set of optics should be selected. Classical lab X-ray diffractometers allow for different optics to be implemented for the incoming and diffracted beams. The optics exchange and realignment generally require some expertise because it implies physical change of some delicate accessories, like X-ray mirrors, or monochromators. However, some of the latest generation of X-ray diffractometers allow for automatic optics exchange between conventional Bragg-Brentano optics, parallel beam optics and even in some cases high-resolution primary optics.

Unlike conventional optics, the shaping and focusing of the X-ray beam is difficult due to small deviation of the refractive index away from unity. Most conditioning of the X-ray beam, therefore, is performed by use of 'shadowing optics', through a series of slits and parallel plates. There are two primary optical modes that diffractometers can be configured in: *Bragg-Brentano optics* and *Parallel Beam optics*.

### *Bragg-brentano optics*

Bragg-Brentano optics, also known as focusing or para-focusing optics, are typically used for powder X-ray diffractometry as a high intensity divergent X-ray beam is used to obtain strong diffraction signals, as shown schematically in **Fig. 5**. The X-ray source and a *receiving slit*, which is positioned in front of the detector, move on a circle (*diffractometer circle*) that is centred on the sample surface. The divergent X-rays impinge on the sample surface at different positions, focusing them back to a single point at the receiving slit. The positions of the source, sample surface, and receiving slit, form a *focusing circle* with a radius that depends on the  $\theta$  angle.

A long metallic slit, known as the *divergence slit*, limits the angular divergence of the X-ray beam, which, by changing the aperture size, is used to change the size of the footprint on the sample. A scattering (or anti-scattering) slit limits the scattered X-rays which do not undergo diffraction from reaching the receiving slit and detector (see **Fig. 5**). Because the Bragg-Brentano mode uses a divergent beam and requires the sample surface to be positioned in the centre of the focusing circle, there are several sources of error one should be aware of:

- A slight misalignment of the sample height,  $h$ , will lead to a shift of the measured peak positions according to  $\Delta 2\theta = 2h \cos \frac{\theta}{R}$ , where  $R$  is the radius of the diffractometer. This is usually the biggest source of error in this mode.
- Because the sample is not curved with the radius of the focusing circle, the sample cannot ever be perfectly aligned with the source and receiving slit. This error is largest when the focusing circle radius is smaller (small  $2\theta$ ) and can be reduced by using smaller divergence slits.
- The footprint of the divergent X-ray beam depends on the incident angle,  $\theta$ . Because X-rays are not diffracted at the surface but have a certain penetration depth which depends on the incident angle, for very thick films, some diffracted X-rays may come from region deeper in the sample which is not aligned on the focusing circle.
- Axial divergence is the angular divergence of the X-ray beam perpendicular to the  $\theta$  and  $2\theta$  axes. This can be minimised by inserting *Soller slits* into the incident and receiving beam optics, which consist of a series of thin parallel metal plates (See **Fig. 5**).

Due to these errors, it is strongly recommended to use Parallel Beam optics for thin films analysis when available.

**Fig. 5** Example of Bragg-Brentano (para-focusing) optics

### *Parallel beam optics*

It is possible to condition the divergent X-rays which leave the X-ray tube to form a parallel beam. This can be done using very small divergent slits in conjunction with parallel plate collimators, which are similar to Soller slits, but with plates rotated by  $90^\circ$ , to further reduce the divergence of the beam. Alternatively, a laterally graded multilayer mirror (parabolic or Göbel mirror) can, through reflection, convert a high proportion of the divergent X-rays to a parallel beam with a divergence of a few  $0.01^\circ$ . [2] As pictured in **Fig. 6a**, the mirror consists of a heterostructure of alternating low-density and high-density layers with a variable layer thickness with distance from the X-ray source according to a parabolic function. This has the advantage of both creating a parallel beam with less significant loss of the X-ray intensity as well as dramatically reducing the  $K_\beta$  component. Since these mirrors are designed for a particular wavelength, they cannot be used with other wavelengths, i.e. a mirror for  $\text{Cu } K_\alpha$  is not effective for  $\text{Co } K_\alpha$ , and vice versa. The mirror needs to be carefully aligned so the optimum incoming angle and position are maintained for all goniometer positions. One interesting feature of X-ray mirrors is that the limited efficiency in reflectivity for a particular wavelength filters out a large portion of the incoming beam energy spectrum, and therefore considerably reduces bremsstrahlung background emission and the  $K_\beta$  line. Unfortunately, typical  $K_{\alpha 1}$  and  $K_{\alpha 2}$  lines are too close in energy to be discriminated by X-ray mirrors and an additional high-resolution monochromator has to be implemented to eliminate the  $K_{\alpha 2}$  contribution (see Box 2). [3]

A typical optics arrangement is shown in **Fig. 6b**, where it should be noted that the divergence in the axial direction is largely unaffected by the use of a mirror and that Soller slits are still necessary to limit the axial divergence of the beam. Another metallic mask (*axial slit*) can be placed after the mirror to control the size of the primary beam, which will limit the illuminated area on to the sample mostly in the axial direction. Other diffractometers may use a set of two cross-coupled parabolic mirrors or a two-dimensional parabolic mirror to produce a fully parallel beam (in two dimensions) while working in point focus configuration. Alternatively, one can use a polycapillary lens, which consists of a long bundle of parallel fibres that turn a diverging beam (in point focus configuration) into a parallel beam with a circular cross-section.

The use of parallel beam optics guarantees that all individual X-ray beams reach the sample with the same controlled incident angle and avoids much of the systematic errors which occur for Bragg-Brentano optics. They are particularly useful for thin film measurements where the film is tilted in  $\omega$  (rocking curves) or  $\psi$  (psi-scans or pole figures), as will be introduced in the next section, which would lead to dramatic defocusing of the X-ray beam if using Bragg-Brentano optics. Parallel beam optics also allow one to perform reciprocal space maps (RSMs) and residual stress analysis, as well as use low incident angles ( $<10^\circ$ ), which opens the door to grazing-incident XRD (see Box 3) as well as X-ray reflectivity

measurements and in-plane measurements, which, although we will not cover in this article, are powerful techniques for thin film analysis by X-rays.

### Attenuators

As the name implies, attenuators reduce the intensity of the X-ray beam reaching the detector. These come in the form of thin metal foils placed in the beam path, and can either be manually inserted or automatically controlled by the computer. As discussed in Section 3.2, if the intensity of X-rays is too high, then the detectors may become saturated and deviate from a linear response or can even become damaged. Therefore, attenuators are vital components for aligning the optics, when a direct beam from the source to the detector is used, or aligning substrate peaks with a high diffracted intensity.

**Fig. 6** (a) Parabolic multilayer (Göbel) mirror (b) example of a parallel beam optics

### Box 2: monochromators

Because X-ray tubes produce the undesirable  $K_{\beta}$  characteristic wavelength, which can impede the correct interpretation of the resulting pattern, some form of chromatic conditioning is always required for XRD measurements. The simplest is an *edge filter*, which is a thin foil inserted into the beam path. These rely on the fact that photoionization of deep electron levels requires a minimum energy, and above this energy the X-rays are absorbed producing a step edge in the transmission function. This can be used to significantly filter out wavelengths below a certain threshold. For Cu anodes, a thin Ni foil significantly reduces the  $K_{\beta}$  contribution (and the  $W L_{\alpha}$  contribution), as shown in Fig. 7 for a 111 diffraction peak of a Si single crystal. Similar results are achievable without Ni filters using newer solid-state detectors, capable of selecting an energy window with a resolution of 380–450 eV.

For higher resolution XRD, single crystals or highly textured polycrystals are used as monochromators. Typical examples are LiF, Si, Ge, and highly-oriented pyrolytic graphite (HOPG), and can either be curved or flat and installed on the incident or receiving optical path. Often when characterising epitaxial thin films, the angular spread of features in the pattern is so small that using both  $K_{\alpha 1}$  and  $K_{\alpha 2}$  will lead to information loss. In this case, we usually use *channel-cut crystal monochromators* to select only the  $K_{\alpha 1}$  contribution. These are a high-quality single crystal of Si or Ge than has been cut so that the X-ray beam diffracts at least twice within the crystal as it passes through the monochromator, as shown in Fig. 7a. They are defined by the crystal used, the diffracting lattice planes, and the number of times the beam is diffracted. The result is a highly monochromatic and parallel beam. The use of a monochromator, unsurprisingly, results in intensity losses, and so the monochromisation method should be selected based on the structural features to be resolved.

**Fig. 7** (a) Schematic diagrams of a 2-bounce and a (Bartel's) 4-bounce channel-cut crystal monochromators. (b) Diffraction peak data of a Si single crystal measured in parallel beam mode (parabolic mirror) using various monochromisation methods. Note the change in intensity for each method. (c) Typical FWHM values one could expect for each monochromisation method

## Methods

### *2 $\theta$ / $\omega$ scan*

The starting point for thin film analysis by XRD is the  $2\theta/\omega$  scan. This is essentially the same type of measurement used in powder diffraction, where the  $\omega$  angle is kept to half of  $2\theta$  or the scattering angle, and the pattern is plotted as a function of  $2\theta$ . During the scan the Bragg plane is always aligned with a crystallographic axis of the substrate and this measurement is often also referred to as a *symmetric* or *coupled* scan.<sup>9</sup>

Prior to performing an  $2\theta/\omega$  scan, the thin film sample must first be aligned to the correct height. Usually, single crystal substrates are used for film growth, which are oriented and cut with a certain crystalline plane parallel to the polished surface. After the sample height alignment, these planes should then be aligned into the Bragg plane. Guidelines for aligning the sample are given in Section 0. Assuming the substrate is perfectly cut, this should result in the surface of the film being aligned into the Bragg plane as well. In almost all cases, however, substrates are not perfectly cut and polished, and so a slight *mis-cut* angle exists between the substrate surface and its crystalline planes. For the sake of simplicity and ease of explanation, in the following sections we will assume that there is no mis-cut and that the substrate lattice is aligned perfectly with the surface, but one should be aware that usually slight mis-cuts are present. If the substrate is polycrystalline or amorphous, then the surface of the film should instead be aligned, as described in Section 0.

During the  $2\theta/\omega$  scan, the Bragg plane is always kept parallel to the surface of the sample, as is the case in a powder diffraction measurement, and so the Bragg condition is fulfilled only for *hkl* planes which are parallel to the sample surface. When measuring powder, however, the crystallites are randomly oriented, and all possible reflections will appear in the diffraction pattern. This is rarely the case for thin films which instead often possess preferential orientation, and so the peaks observed will depend not only on the phases present, but also on their orientation.

<sup>9</sup> Sometimes other notation will be used that refers to similar types of measurement but with key differences. A  $\theta/2\theta$  scan is a symmetric or coupled scan about the surface normal of the sample and plotted as a function of  $2\theta$ , which is most commonly used in power diffraction measurements. A  $\omega/2\theta$  scan is a symmetric or coupled scan about the crystallographic axis of the substrate, but plotted as a function of the  $\omega$  angle.

Note this, because it is a very important detail that is often disregarded or misinterpreted when analysing thin films.

Slight shifts in the peak positions in the  $2\theta/\omega$  scan is common due to residual stresses, substrate induced strain, or compositional changes in the film. The shape of the peaks is determined by the size of the grains, as well as compositional gradients and strain distributions. Details on peak fitting are given in Section 0. Due to the almost perfect nature of single crystals, peaks from the substrate will often dominate the pattern,<sup>10</sup> whereas peaks from the film may be very low in intensity due to the much lower film thickness. Accordingly, it is common to plot patterns from thin films on a logarithmic intensity scale.

**Fig. 8** shows several examples of diffraction patterns from epitaxial, textured, randomly-oriented polycrystalline, and amorphous films. In some cases, these descriptions of films can be rather ambiguous, so in the following we explain what is meant for each case, and what one could expect in an  $2\theta/\omega$  scan.

- *Epitaxial films:* This can refer to almost 'perfect' growth where a film is essentially a single crystal in perfect registry with the substrate, such as achieved in semiconductor films on Si wafers. As the quality of the epitaxy decreases, misfit or edge dislocations at the interface with the substrate may be present as well as threading dislocations through the film, connecting the misfit dislocations with the surface. A further decrease in the epitaxial quality may result in mosaic domains, each in good registry with the substrate, but separated by low angle grain boundaries. All of these cases can collectively be called epitaxial growth, but of varying quality. For an epitaxial film, one would expect to see a single set of peaks in the pattern from the film according to a single orientation, as shown in **Fig. 8a**. For a film to be designated epitaxial, the lattice planes must be well-aligned both in-plane and out-of-plane (biaxially), and so it should be noted that a  $2\theta/\omega$  scan does not give enough information by itself to ensure the film is fully epitaxial, as the reflections which are observed only depend on the out-of-plane orientation (a monoaxially oriented film may look the same in the  $2\theta/\omega$  scan). Pole figures or  $\phi$ -scans are still needed to assess the in-plane orientation.
- *Textured films:* Any film with an anisotropic distribution of crystallites is said to be textured or have preferential orientation. In the  $2\theta/\omega$  scan, texture can be recognised as an enhancement of the relative intensity of some Bragg reflections and a reduction of others (shown in **Fig. 8b**), as compared to a powder diffraction pattern of the same material. The most extreme example of this would be an epitaxial film, as described above. Texture can be due to templating from the crystalline orientation of the substrate, minimising the surface energy during deposition, or the competition between surfaces with anisotropic growth rates from grains with different orientations. Preferential orientation may exist both out-of-plane and in-plane with respect to the substrate crystal axis, or may be mono-axially textured out-of-plane and randomly oriented in-plane (fiber-texture). When

<sup>10</sup> Be careful not to oversaturate the detector. Use an attenuator if necessary.

texture is observed in the  $2\theta/\omega$  scan, it is usually necessary to perform pole figures or  $\phi$ -scans to assess the in-plane orientation to build a full picture of the film orientation.

- *Randomly-oriented polycrystalline films:* Polycrystalline films with no preferential orientation should display the same number of peaks with the same relative intensity as the powder diffraction pattern. An example of such a film is shown in **Fig. 8c**. Because films are often much thinner than the penetration depth of X-rays, reflections from randomly oriented films can be very weak, and often less-intense peaks are not observed at all as they are lost in the background noise. For films with this structure, grazing-incidence XRD is recommended, as described in Box 3.
- *Amorphous films:* Films grown at lower temperatures may result in the formation of amorphous phases. As XRD relies on a well-defined periodic crystalline structure, as demonstrated in Figure 1, amorphous films are naturally more difficult to characterise, and often essentially invisible in  $2\theta/\omega$  scans. Although amorphous films lack long range order, they do possess a degree of short-range order, which may be observed by XRD. If such a film is thick enough, very broad, low intensity, peaks may be observed, as seen in **Fig. 8d**, in contrast to the sharp peaks seen in crystalline materials.

From these examples, it should be clear that the symmetric  $2\theta/\omega$  scan is an indispensable tool in thin film analysis. It does not require a Euler cradle, and can be performed with either Bragg-Brentano or Parallel beam optics, although from our discussion in Section 3.4, Parallel beam optics are recommended if available. Guidelines on sample alignment, choosing the scan parameters, and details on peak fitting and data analysis are given in Sections 0 and 0.

**Fig. 8** Example  $2\theta/\omega$  patterns for (a) an epitaxial film, (b) a textured film, (c) a randomly-oriented polycrystalline film, and (d) an amorphous film. The insets show schematics of the microstructure. All the patterns show a sharp, intense grey peak exemplifying the contribution of the single crystal substrate

### **Box 3: grazing-incidence XRD (GIXRD)**

The penetration depth of X-rays is in the 1-100  $\mu\text{m}$  range, and because films are often substantially thinner, the substrate diffraction peak typically dominates the resultant pattern. The intensity of reflections from randomly-oriented polycrystalline films is often particularly low, as only a subset of the grains is contributing towards the signal. In GIXRD, the incidence angle,  $\omega$ , is fixed to a small angle of approximately  $0.5\text{-}1^\circ$ , slightly above the critical angle (below which total reflection will occur), and the detector is moved on the  $2\theta$ -circle to collect the pattern. In this way the penetration deeper into the sample is considerably reduced and the intensity of the film peaks is enhanced with respect that of substrate.

It is important to note that during the scan the Bragg plane no longer remains parallel with the surface of the film and instead moves as  $2\theta$  is varied. GIXRD is, therefore, better suited for samples without a preferential out-of-plane orientation, where the resultant pattern should yield peaks at the same  $2\theta$  angles as would be found in a symmetric  $2\theta/\omega$  pattern. For highly-oriented samples, peaks will often not be observed, or if present, may provide information of any existing randomly oriented weak contributions from the surface, interface, or intragranular components. GIXRD requires particular optics, with a parallel beam, very small incidence slit, and a parallel plate collimator in the diffracted beam, as shown in **Fig. 9**. By varying the incidence angle, it is possible to systematically change the X-ray penetration depth in the films and extract depth-resolved structural information. The alignment of the sample and analysing the pattern are similar for the  $2\theta/\omega$  scan and are covered in Sections 0 and 0.

**Fig. 9** Example of grazing-incidence optics

#### *Rocking Curve ( $\omega$ scan)*

In a rocking curve, the Bragg angle,  $2\theta_B$ , is fixed to the centroid position of a particular reflection in the  $2\theta/\omega$  scan, and the sample is tilted (or 'rocked') in the  $\omega$  axis such that planes no longer parallel with the sample surface are brought onto the Bragg plane. This is visualised in **Fig. 10**. This result is a single bell curve, known as a rocking curve, which gives the distribution of planes as a function of tilt. The width of the rocking curve depends upon the mosaic spread of the grains, density of dislocations, and substrate curvature, which disrupt the parallel nature of the lattice planes. Therefore, the full-width half-maximum (FWHM) of the rocking curve is often recorded and is generally used as an indication of the quality of intended epitaxial growth, or indication of preferential orientation. One should be careful to not mix up the width of the rocking curves with the widths on the peaks in the  $2\theta/\omega$  scan, as each provide very different information.

As one might expect, rocking curves are particularly useful for epitaxial or textured films, but would yield little information for randomly-oriented polycrystalline or amorphous films. A highly oriented film, for instance an epitaxial film or a film with dominant columnar growth, generally shows a Gaussian type curve with full width half maximum (FWHM) from a few tenths of a degree to a couple of degrees, while a more disoriented film may show a broadening of several degrees. A randomly oriented film would show a constant intensity independent of the  $\chi$  angle simply because there is the same probability of finding crystallites in any direction. In practice, there could be some variations in intensity at large tilt angles because of changes in the illuminated area as well as in X-ray absorption.



A common strategy is to first perform a  $2\theta/\omega$  scan, followed by rocking curves on each of the observed diffraction peaks. As with the  $2\theta/\omega$  scan, a Euler cradle is also not necessary for rocking curves, only a diffractometer where the incident and detector angle can be decoupled. Parallel beam optics are usually necessary for rocking curves due to the beam defocusing which occurs for a divergent beam as the sample is tilted. The minimum width of a rocking curve that can be measured will depend on the optics used and is limited by the primary beam divergence. Highly epitaxial films require high resolution optics (primary beam 2- or 4-bounce crystal monochromator).

**Fig. 10** (a) Schematic of a rocking curve measurement and (b) example of resultant rocking curves from a film and substrate diffraction peak. Note that this is drawn from the reference frame of the sample; depending on the diffractometer either the sample or source and detector are 'rocked' during the scan

### *Pole figures*

During  $2\theta/\omega$  scans and rocking curves, only the planes parallel or close to parallel with the surface are measured. At most this can only give us the orientation of the film in the out-of-plane direction but could not be used to distinguish between texture in all three principle axes of the films and fibre-texture. To assess the in-plane orientation, it is necessary to tilt and rotate the sample in order to move lattice planes which are not parallel to the surface into the Bragg plane. This is performed as a *pole figure* using the  $\psi$  and  $\phi$  axes via a Euler cradle.

Prior to performing a pole figure measurement, the sample must first be aligned such as for the  $2\theta/\omega$  scan, then the  $\omega$  and  $2\theta$  axis set to the Bragg angle of a particular reflection of the film. This does not necessarily need to be one which appears in the  $2\theta/\omega$  pattern, and it is often beneficial to perform pole figures on planes which are not parallel with the surface. The sample is tilted in incremental steps in  $\psi$ , and rotated a full  $360^\circ$  in  $\phi$  for each step. Planes with a d-spacing corresponding to the Bragg angle will cause diffraction as they are tilted and rotated into the Bragg plane, yielding an intensity map as a function of tilt and rotation angle. The intensity map is easy to visualise from the sample reference frame as a hemisphere, as shown in **Fig. 11**. Planes which satisfy the Bragg condition appear where the plane normal intersects the hemisphere surface. Pole figures are generally represented as a circle; using polar coordinates with  $\psi$  as the radial coordinate, and  $\phi$  as the angular coordinate.

**Fig. 11** (100), (110) and (111) poles of a cubic crystal on a hemisphere, representing the  $\psi$  and  $\phi$  axes scanned during a pole figure measurement

When carrying out pole figure measurements for the first time, it can be difficult for the beginner to visualise the information in the pole figure and to understand how it relates to the crystal orientation. To help with this, **Fig. 12** shows schematic

examples of a (001) and (111) out-of-plane oriented films with a single in-plane orientation, and example pole figures from the 001, 011, and 111 Bragg reflections. For simplicity, both are for cubic systems. The  $\psi$  angles at which certain reflections will appear are given by the *interplanar angles*. The interplanar angles for a cubic system are given in Table S2 of the supplementary information. Peaks will appear at an  $\psi$  angle between the out-of-plane orientation and the Bragg reflection corresponding to the  $2\theta$  angle. For example, if a film is (001) oriented out-of-plane, and  $2\theta$  is set to the Bragg angle of the (111) planes, then peaks will appear at  $\psi = 54.7^\circ$ , as shown in Fig. 12d. The number of peaks in the azimuth for a given  $\psi$  angle will depend on the crystal symmetry for the particular  $hkl$  reflection and the number of distinct in-plane variants. For the example in Fig. 12d, four maxima at  $\psi = 54.7^\circ$ , equally spaced in the azimuth are observed for a single in-plane orientation. For two in-plane variants related by a  $45^\circ$  in-plane rotation, this would be observed as eight maxima. For an out-of-plane orientation along the 001 axis and no preferential in-plane orientation (grains free to rotate in  $360^\circ$  of freedom), a continuous ring at  $\psi = 54.7^\circ$  would be seen. Fig. 12f,g,h show the case for an out-of-plane (111) oriented film, with pole figures taken from the 001, 110, and 111 reflections, respectively. As before, the number of maxima in each pole figure is for a single in-plane orientation; if more reflections are observed or a continuous ring, then this is indicative of more than one in-plane orientation for fibre texture, respectively.

**Fig. 12** Example pole figures for a (a) (001) out-of-plane oriented film and (e) (111) out-of-plane oriented film. Pole figures from the (b, f) 001 Bragg reflection, (c, g) 011 Bragg reflection, and (d, h) 111 Bragg reflection

Pole figure measurements are mostly suitable for textured samples, which display preferential out-of-plane orientations in the  $2\theta/\omega$  scan, and therefore require the in-plane orientation to be assessed. It is often necessary to perform pole figures around several Bragg reflections to build up the full orientation distribution. Usually the orientation of the film is given with respect to the substrate, and it is therefore necessary to perform at least one pole figure measurement on a reflection of the substrate. For accurate determination of the orientation relationships, it is best to perform all the pole figures on the film and substrate reflections without removing the sample from the diffractometer to ensure the  $\phi$  axis is identically aligned with respect to the sample for all measurements. Pole figures can also be useful for determining the crystal symmetry of a film, when only a limited number of reflections appear in the  $2\theta/\omega$  scan due to preferential orientation. For example, cubic and tetragonal crystal structures yield distinctive pole figures, even if the phases cannot be distinguished in the symmetric  $2\theta/\omega$  scan.

Tilting the sample during pole figures causes defocus of the X-ray beam if Bragg-Brentano optics are used, which causes peaks to become broader and shift in  $2\theta$  as a function of  $\psi$ . Therefore, parallel beam optics are, if available, recommended for pole figure measurements, although peaks may still shift as  $\psi$  is varied due to residual stresses in the film. If para-focusing optics are to be used, either point-focus or a slit perpendicular to the X-ray beam (Schulz slit) and a narrow

divergence slit should be employed to minimise the divergence of the incident beam, and a larger receiving slit used to capture maximum intensity of the diffracted beam for broad or shifting peaks. It should be obvious that pole figures cannot be measured out to  $\psi = 90^\circ$ , and for Bragg-Brentano optics, a maximum of  $\psi = 70^\circ$  is typical. Parallel beam optics may allow for a maximum of  $\psi = 85 - 89^\circ$ . If the information required lies outside the  $\psi$  range, it is possible to take pole figures at a different scattering angle where the crystallographic planes appear at an appropriate tilt angle. For example, pole figures of the 001 reflection of a (001) out-of-plane oriented film will lead to maxima at  $\psi = 0^\circ$  and  $\psi = 90^\circ$ , whereas a pole figure of the 111 reflection will display maxima at  $\psi = 54.7^\circ$ . The selection of  $hkl$  reflections should also avoid, if possible, any overlap with substrate peaks, as their high intensity may dominate the pole figure. For strongly epitaxial films, where the lattice parameters of the substrate and the film are closely matched and both have the same crystal symmetry, peak broadening causes the substrate to dominate the pole figure and little information can be extracted. In this case, higher resolution optics are recommended, in order to minimize overlap, and it may be better to perform simpler measurements such as a combination of rocking curves (Section 0) and phi-scans (Section 0) to obtain information about the overall film texture.

Point-focus is recommended for both parallel and para-focusing optics due to the increase in beam footprint on the sample surface at high tilt angles. If the X-ray beam footprint on the sample becomes larger than the sample surface due to tilting during the measurement, geometric effects due to the shape of the sample can influence the pole figure. For example, many substrates for thin film growth are square and will lead to varying intensities as the sample is rotated in the azimuth. It may be possible to correct for these effects by performing a linear background subtraction by remeasuring the pole figure for scattering angles above  $(2\theta_B + \Delta)$  and below  $(2\theta_B - \Delta)$  the peak position and subtracting the average of both scans.

#### *Azimuth Scans ( $\phi$ Scans)*

In some cases, a full pole figure or series of pole figures are not necessary and instead one may simply opt to move the diffractometer to a certain Bragg reflection,  $2\theta_B/\omega$ , tilt the sample in  $\psi$  corresponding to a particular interplanar angle, and scan while rotating the sample,  $\phi = 0 - 360^\circ$ . This is known as a  $\phi$  scan. The number of maxima observed during a  $\phi$  scan will depend on the Bragg reflection, out-of-plane orientation, and number of preferential in-plane orientations of the grains in the film. Examples are shown in **Fig. 13** for a cubic (001) out-of-plane oriented film with a single in-plane orientation. **Fig. 13a** shows a  $\phi$  scan taken for the 110 reflection ( $2\theta_B$  angle) at  $\psi = 45^\circ$  and **Fig. 13b** shows a  $\phi$  scan taken for the 111 reflection at  $\psi = 54.7^\circ$ . Both show four peaks, which due to the crystal symmetry and out-of-plane orientation of the system, indicates a single in-plane orientation.

The advantage of  $\phi$  scans over pole figures, is that they are much quicker to perform if the information required is straight-forward.<sup>11</sup> The same considerations of beam divergence with tilting as discussed in Section 4.3 must still be taken into account, and full pole figures may still be preferred for more complex systems.

**Fig. 13** Schematic  $\phi$  scans for a cubic (001) oriented film for the (a) 110 reflection at a  $\psi = 45^\circ$  and (b) 111 reflection at  $\psi = 54.7^\circ$

## Guidelines for measurements

In this section, we give practical guidance on carrying out XRD analysis of thin films. Prior to measuring, the appropriate optics arrangement must be selected and aligned, the sample must be aligned in the diffractometer, and the scan conditions must be designated. Software to control the diffractometer may be significantly different depending on the instrument manufacturer, and here we will assume the reader is able to control the instrument. One should be aware that in some cases different manufacturers will use slightly different notation for the angles, optical components, measurement methods, but the fundamental principles as presented here will still apply.

### *Choosing the right optical mode*

Parallel beam optics are strongly recommended for XRD analysis of thin films if available. The sources of error due to beam divergence for Bragg-Brentano optics, as discussed in Section 0, can be largely minimised by using a parallel incident beam. Beam divergence can be particularly problematic for measurements where the sample is tilted in the Bragg plane such as rocking curves and pole figures. Bragg-Brentano optics may be desirable for symmetric  $2\theta/\omega$  scans where the highest possible intensity of X-ray is required for observing weak peaks; but if a Göbel mirror is available then a parallel beam can be employed with minimal decrease in the intensity and is the preferred choice.

Line-focus should be used for  $2\theta/\omega$  scans and rocking curves to maximise the area of the film exposed to the beam. An axial slit should also be used to limit the width of the beam to less than the size of the sample. For pole figures or  $\phi$  scans, point focus is recommended if possible, as the tilting of the sample in  $\psi$  leads to a dramatic increase of the footprint and defocusing of the beam. Point focus can either be achieved by re-orienting the source to align one of the point-focus windows (as seen in **Fig. 3b**) or using axial and divergent slits.

The choice of monochromisation method to use will depend on the structural features to be resolved. There is always a trade-off between the intensity of the

<sup>11</sup> 2D detectors, which are becoming increasingly available, are capable in collecting a large  $\psi$  and  $2\theta$  range for a single  $\phi$  scan. These can dramatically reduce the time needed to perform certain measurements, such as pole figures.

beam and the angular resolution, and so it is best to use the method that maximises the X-ray intensity while still ensuring that no necessary information is lost (see Box 2). Here we will not describe the procedure for exchanging and realigning the optics as the procedure may be different depending on the make and model of diffractometer. It is best to consult the manager of the XRD equipment on the available optics and how to install them.

A quick and useful check to ensure the optics are not misaligned is to set the  $2\theta$  axes to  $0^\circ$  (so that the X-ray beam is pointed directly at the detector) and to perform a  $2\theta$  scan around this point to ensure the direct beam is centred at  $0^\circ$ . Because this involves the direct, undiffracted beam being directed onto the detector, it is very important that an attenuator is used to prevent damage to the detector. One important point to note is that the optics alignment and alignment check should be carried out at the tube voltage and current that will be used for the measurements, as changes in the current or voltage can lead to slight differences in the beam shape as it emerges from the X-ray tube.

### *Positioning and aligning the sample*

Once the optics for a particular measurement is set and aligned, the film to be measured can be placed on the sample stage. In some diffractometers the sample stage is horizontal, while in others it is vertical and so the film must be held down, often with adhesive tapes or glues. One should ensure that the sample is properly centred and flat.<sup>12</sup> It is important to make sure that no other contributions from a material holding the sample (any screws, clips, adhesive tape), or the sample stage material are crystalline such that they give some contributions to the scan. If these are unavoidable it is necessary to know their possible contribution by measuring them without the sample present. Typically, samples can be mounted on a glass plate (a microscope slide is a good option) by using some adhesive tapes or glues which do not give significant peaks (double sided carbon tape as used with a scanning electron microscope is often suitable). It is good practice to limit the axial size of the beam to less than the width of the film to avoid any contributions from tape or adhesive used to fix the sample in place, or deviations from homogeneity expected at the film edges.

When the film has been positioned on the sample stage, the film must be precisely aligned to the correct height (z axis) and to ensure the sample surface is parallel with the Bragg plane. This is particularly critical when using Bragg-Brentano optics

---

<sup>12</sup> Some sample stages are equipped with a x- y- z stage which allows for several samples to be placed together depending on their size. When placing several samples, one has to be aware of, or limit, the illuminated area with the corresponding set of slits and masks so one sample is illuminated at a time and none of the rest of the samples interferes in the measurement. It is a common practice not to place the samples in close proximity (leave at least 1 cm spacing between samples) and try to place them, if possible, at similar height (z-plane). The z-position and surface alignment should be carried out separately for each film.

or in case of low  $2\theta$  angle measurements<sup>13</sup>. The z-position can be adjusted optically (using a laser) or mechanically by using a proper gauge which has previously been calibrated to bring the sample surface to the goniometer centre. Often the best choice, however, is to align the sample by bisecting the direct X-ray beam where the z-axis and  $\omega$ -axis are varied while monitoring the intensity at the detector. This is independent of any possible misalignment of the goniometer for the selected optics.

1. Set  $2\theta=0^\circ$  to direct the X-ray beam at the detector.<sup>14</sup>
2. Run a scan of the z-axis, which should result in a step function as shown in **Fig. 14a**, and set the z-position to where the intensity is half the maximum, bringing the sample to the correct height.
3. Next, to ensure the sample surface is parallel to the beam, run a scan of the  $\omega$ -axis, which should result in a broad triangular-shaped peak, and set the  $\omega$ -angle to the peak maximum as shown in **Fig. 14b**.
4. Continue running consecutive z-axis and  $\omega$ -axis scans (repeating steps 2 and 3) until there are no changes in the resultant profiles. The height of the maxima should now be at half the direct beam intensity,  $I_{\max}/2$ .

The sample surface should now be aligned in the Bragg plane. Often, the  $\omega$ -axis position is not centred on  $0^\circ$ , and it may be necessary to enter an  $\omega$ -offset into the software to account for the difference.

**Fig. 14** Example (a) z scan and (b)  $\omega$  scan at  $2\theta=0^\circ$  for aligning the sample to the correct height in the diffractometer. The dashed lines show the position the diffractometer should be set to

For pole figures and  $\phi$  scans, or when working with amorphous or randomly oriented polycrystalline films, the sample surface alignment described above is usually sufficient before starting a measurement. When working with textured or epitaxial films, the orientation of the planes may be very pronounced such that slight tilt of the sample of some tenths of a degree could make the intensity of the reflections decrease significantly because the planes are no longer in the Bragg condition. It is important, therefore, to carefully align the sample so the intensity of the peaks is maximum.<sup>15</sup> An out-of-plane substrate peak is usually the best choice to align into the Bragg plane, as they tend to be very narrow and the diffracted signal from the substrate is more intense than for a film peak.<sup>16</sup> To perform this alignment:

<sup>13</sup> Precise sample height and surface normal alignments are particularly crucial for grazing incident measurements, for example X-ray reflectivity (XRR) or in-plane diffraction.

<sup>14</sup> Remember to use an attenuator!

<sup>15</sup> This is also particularly important if there is a miscut angle between the planes of the substrate and film and that of the surface normal, which is aligned using z-axis and  $\omega$ -axis scans. The miscut angle can vary from a few tenths of degrees to some degrees in vicinal substrates. This angle will also vary depending on the rotation of the single crystal surface via the azimuthal axis ( $\psi$ ).



<sup>16</sup> Since the penetration depth of X-rays is much larger than the typical thickness of films which are generally below a few microns, the diffracted signal from the substrate is more

1. Fix the detector  $2\theta$  angle to the known position of the substrate crystal cut  $hkl$  plane (a list of peak positions for commonly used crystal substrates and orientations is given in the Supplementary Information).
2. Set the  $\chi$ -axis to half the  $2\theta$  angle. Scan the  $\chi$ -axis and set the diffractometer position to the peak maxima.
3. Scan the  $\psi$ -axis and set the diffractometer position to the peak maxima.
4. Repeating steps 2 and 3, the  $\chi$ - and  $\psi$ - axes be consecutively scanned, until the peaks do not shift by more than  $\pm 1\%$ . It is worth periodically scanning the  $2\theta/\omega$  axis to ensure the  $hkl$  peak has not shifted during the alignment.<sup>17</sup>

Note that the shape of the peak in a  $\chi$  scan can be very narrow (typically below 0.5-1 degree). However, a scan in  $\psi$  angle is usually very broad when using typical line focus geometry as a result of the large divergence on the primary beam in the axial direction. The optimisation is valid for a particular  $\omega$  angle (sample rotation). Any change in  $\omega$  would require a new  $\chi$  and  $\psi$  optimisation. Generally, film planes are oriented relative to the substrate planes, so the substrate reference is valid for film planes too. However, there could be some special cases where film strain relaxation processes produce a slight tilt between substrate and film planes. In those cases, a more accurate measurement is needed.

#### *Choosing scan conditions*

In general, the scan conditions will depend on the characteristics of the films to be measured and the diffractometer being used, and is therefore something that can be gradually optimised over time as one gains experience working with the instrument and certain types of film. Below is a list of some of the considerations that should be taken into account when setting up a measurement. Box 4 gives a set of initial scan conditions to get started with or when working on unknown film samples.

-  **Slits and apertures:** For Bragg-Brentano optics the divergence and receiving slit will control the beam divergence and must therefore be selected depending on the angular features to be resolved while ensuring sufficient beam intensity. For parallel beam optics, the divergence slit will primarily be used to change the size of the beam footprint on the sample. For both optic modes, an axial slit should be used that is smaller than the width of the film being measured.
-  **Scan range:** This should obviously be large enough to include the peaks of interest and necessary information expected from your film and substrate. If these are not known, then wide scans, as given in Box 4 are usually sufficient to cover the main reflections of most oxide materials.

---

intense than for film peaks. The exceptions being for grazing incidence geometries, highly absorbent materials, and very thick films. If the substrate peaks are not present or very weak, then aligning the sample using the film peaks is advisable.

<sup>17</sup> Some commercial single-crystal substrates might not have the expected quality, and display peak splitting in the  $2\theta/\omega$ ,  $\omega$ , and  $\psi$  alignment, which implies twinning or multiple crystal domains are present. In this situation, it is usually best to align to the most intense peak.

- *Number of steps/increments:* In order to accurately fit the position and shape of a peak there should be at least 10 data points over the FWHM range. The step size will therefore depend on the features in the films and on the monochromisation method used.
- *Scan speed:* Often it is desirable to minimize the time taken to perform a scan while ensuring sufficiently high-quality data, in order to maximise productivity when using the diffractometer. As a rule of thumb, the signal-to-noise ratio should be about 3-5 for the smallest peaks and features in the resultant data. Depending on the instrument, sometimes steps/second is used and for others degrees/minute. The optimal time taken to perform a scan will depend drastically on the source intensity, optics, detector, and type of film being measured.

#### **Box 4 Initial scan conditions**

When starting out or working with a new type of film for the first time, it can be difficult to know where to start when choosing scan conditions. Below is list of conditions for each type of measurement introduced in this paper, which may serve as a basis for future refinement.

##### 2 $\theta$ / $\omega$ scans (or GIXRD)

- Scan range: 2 $\theta$  from 10 to 100°
- Step size: 0.03-0.01° (without a crystal monochromator) or 0.001° and lower (with a crystal monochromator)
- Scan speed: 1 degree/minute

##### Rocking curves

- Scan range:  $\omega$  from -5° to 5° about the 2 $\theta_B$ /2 position
- Step size: Same as 2 $\theta$ / $\omega$  scan
- Scan speed: Same as 2 $\theta$ / $\omega$  scan

##### Pole figures

- Scan range:  $\psi$  from 0° to 80°;  $\phi$  from 0° to 360°
- Step size: 5° for both  $\psi$  and  $\phi$  (should be kept the same for both axes)
- Scan speed: About 30-60 mins for the full pole figure

##### $\phi$ Scans

- Scan range:  $\phi$  from 0° to 360°
- Step size: At least 5 data points within a peak
- Scan speed: About 30-60 mins for the scan

## **Analysing the data**

Most diffractometers come with software for analysing the XRD data from the various types of measurement. Common graph plotting or spreadsheet software is also capable for the analysis presented below. Box 5 contains a selection of frequently asked questions often encountered when starting out analysing XRD data from films.



### *Analysing $2\theta/\omega$ scans*

Typically for  $2\theta/\omega$  scans, the substrate peak will dominate the pattern and so it is almost always better to plot the results on a logarithmic scale to ensure that all the reflections from the film are visible. For powder diffraction, all the  $hkl$  reflections are visible in the pattern and so it is common to fit the full pattern to yield information on the crystal structure.<sup>18</sup> Because most films have some degree of preferential orientation, only a selection of  $hkl$  planes that are aligned with the surface are visible in the scan and so analysis is often based on fitting the peaks individually. There are three things that must be considered when analysing the data from  $2\theta/\omega$  scans: (1) Which peaks are present? (2) What are the precise peak positions? (3) What are the shapes of the peaks?

### *Presence of peaks: Phase identification and texture*

The presence and absence of peaks in a pattern give information on both the phases present in the film and on the orientation. As films are often textured and only a subset of the crystallographic planes is observed, this can sometimes make assigning the phases and orientations challenging. Furthermore, slight shifts in the peak position due to residual stress, non-stoichiometry, or compositional changes (as discussed below) can also hinder identification.

The pattern taken of the film should be compared against powder diffraction patterns of materials and phases that are expected to be present in the film. If the film was grown from a stoichiometric target (using PVD techniques such as pulsed laser deposition, radio-frequency sputtering, or electron-beam evaporation) then comparing to a powder pattern of the parent material is recommended. Alternatively, if this is not available, or there are phases in the film which are not present in the parent material, there are several databases available which contain vast libraries of single-phase XRD powder patterns for comparison.<sup>19</sup> These give the  $d$ -spacings,  $2\theta$  position (for a given wavelength), and relative intensities for the  $hkl$  planes.<sup>20</sup>

---

<sup>18</sup> The La Bail and Rietveld refinement methods are powerful techniques for determining the crystal structure from powder diffraction methods, but have limited use for thin film analysis.

<sup>19</sup> Databases of crystal structures of inorganic materials that can be used to generate powder diffraction patterns are available, such as the Inorganic Crystal Structure Database (ICSD), the International Centre for Diffraction Data (ICDD), and the Crystallography Open Database (COD), the latter of which is free to access.

<sup>20</sup> When selecting reference patterns from a database, it is important to check the conditions under which the data were obtained that was used to calculate the reference crystal structure. Some structures come from XRD data taken at high temperatures, high pressures, or reducing conditions, and others come from simulations. It is also worth bearing in mind the reliability and precision of the diffraction data used to calculate the

When indexing the peaks from a thin film it is important to pay attention to the relative intensities as well as the expected peak positions. Even if the pattern from a film displays all the peaks from the powder pattern, if the relative intensities of the peaks is not the same as the powder pattern, then there is some degree of texture in the film.<sup>21</sup> Another useful check when assigning a peak to a certain  $hkl$  plane is to check for high-order reflections within the scan and compare the relative intensity between the two peaks with that of a powder diffraction pattern. For example, if one peak in the film pattern is assigned to 001, then the 002 peak should also be visible (if within the scan range), and the relative intensities should be the same as a powder pattern as the peaks are coming from the same family of planes.

When analysing the texture, it is important to bear in mind that the  $2\theta/\omega$  scan only gives information from planes parallel with the surface. A single orientation observed in a  $2\theta/\omega$  scan does not necessarily imply perfect epitaxial growth with the substrate, and often multiple in-plane orientations are present. If preferential orientation in the film pattern is observed, often pole figures or azimuth scans are needed to build up a full picture of the texture.

### **Box 5 Frequently asked questions**

#### Is my film textured?

Compare the  $2\theta/\omega$  scan to a powder diffraction reference. Are all the peaks present? Do the relative intensities match the reference pattern? If the answer to either question is “no” then the film has some degree of preferential orientation and rocking curves and pole figures/ $\phi$ -scans should be performed to build up a full picture of the texture.

#### I can't identify this peak!

If a peak cannot be assigned to the parent material or reference pattern, check for other X-ray wavelengths (Cu  $K_\beta$  or W  $L_{\alpha 1}$ ; **Table 1**) that might be diffracting off strong film or substrate  $hkl$  planes. To check for any contributions from the sample holder, stage, or adhesive tape run a blank substrate with no film present.

#### Why are my peaks shifted to a different $2\theta$ ?

First check the substrate peak positions or reference sample to ensure the diffractometer is not misaligned. If not, the lattice parameters of the film may have changes due to compositional strain, epitaxial strain, thermal strain, or intrinsic residual strain. Frequently, oxide films are reduced as deposited leading to chemical expansion, and it is often necessary to anneal them in oxidising atmospheres to ensure oxygen stoichiometry. Performing further XRD experiments such as reciprocal space mapping (RSM), residual stress analysis, and

---

structures. Some databases have an indicator for the quality of the data the structure is calculated from.

<sup>21</sup> Although this is generally the case, in some instances, there may be subtle changes in the crystal symmetry that affects the structure factor and relates to changes in relative intensities of the peaks. In some layered compounds changes in the stacking sequence during film growth can cause the absence of some peaks, which may be erroneously interpreted as preferential orientation. If in doubt, performing rocking curves of the reflections present should allow one to determine the orientation of the domains.

in-plane diffraction may be necessary understand the full nature of the strain for a given film.

Why are my film peaks surround by a bunch of fringes?

Fringes may form to the left and right of strong film peaks and are characteristic of X-ray diffraction of a perfect crystalline sample with a finite size. These often occur when using high-resolution optics on thin films and multilayers with a thickness of around 100 nm and lower. The spacing between the fringes relates to the 'coherent size' of the sample, normally corresponding to the total thickness. The appearance of fringes is an indication of the crystal quality of the film, as the presence of local distortions (dislocations, local point defects, interface and surface roughness) blurs the fringe patterns. The combined peak and fringes can be fitted using software provided by most of the diffractometer manufacturers. More information of the theory behind these phenomena can be found in Refs. [3, 8, 9]

Why are my peaks asymmetric?

It could be due to a distribution of lattice parameters due to compositional or strain heterogeneities, or the superposition of two reflections, but it is worth checking the film was correctly aligned in the diffractometer. Also, edge filters (see Box 2) can cause asymmetry and shoulders to appear on intense peaks.

Why does my  $2\theta/\omega$  scan not show any film peak other than substrate peaks?

Either, i) the film material is highly oriented but the sample was not properly aligned in  $\chi$  (re-do the alignment; it is also possible that film peaks might be slightly tilted from substrate orientation), ii) the film peaks match perfectly those of the substrate, (ultra-high resolution measurement is needed to resolve film and substrate contributions), or iii) the film is polycrystalline, amorphous, and/or consists of light elements so the intensity of the film peaks are very low (probably a GIXRD measurement is needed).

Why are there some additional peaks corresponding to forbidden reflections for a given space group?

It could be that strain could slightly modify the structure resulting in a symmetry of a different space group. In some cases substrate intense reflections could also generate some multiple scattering effects inducing the appearance of new "Bragg" peaks, (such as for instance the "200" reflection in Si (100) single crystal wafers).

*Precise peak positions: Lattice parameters - strain and composition*

The peak positions in the  $2\theta/\omega$  scan will relate to their corresponding out-of-plane interplanar distances. Any variation in the positions with respect to the parent materials (or reference pattern from a database for similar measuring conditions: temperature, atmosphere, total pressure) may be interpreted in terms of different sample characteristics,[4] either: i) variations in the chemical composition, often called chemical strain (which may include deviations during film growth, even interdiffusion with substrate elements, or changes in the stoichiometry of lighter elements during postprocessing); ii) variations in cell parameters due to a certain elasticity of the material to adapt to the substrate cell parameters, called epitaxial strain; or iii) variations in the cell parameters due to a different thermal expansion coefficient of substrate and film when growing at elevated temperatures, called thermal strain, (also induced by phase transitions occurring during cooling down

process); or iv) some residual strain induced by the thin film deposition conditions or post-processing when using highly energetic particles, typically in physical deposition methods like sputtering or ion implantation, caused by the particle impingement, often call intrinsic residual strain.

There are special cases, when the thin film sample is a composite, where the matching between the two structures at their interfaces produces an additional source of strain, which may modify the cell parameters of one, or both of the phases in the sample. In ultrathin films, or in thin film regions close to the substrate interface or the film surface, proximity effects may generate an induced electrostatic (or magnetic) field, which may induce some subtle cell expansion by electrostriction (or magnetostriction). It is also worth bearing in mind that domain tilt or sample tilt (if not properly aligned) can lead to slight variations in the peak position.<sup>22</sup> If in doubt, perform a rocking curve measurement of the peak to check if it is centred on  $2\theta_B/2$ .

For very accurate measurements of the cell parameters, the peaks in the pattern should be fitted with a pseudo-Voigt function to precisely determine the maxima. To account for any instrumental errors such as the zero-shift, height misalignment, curvature, or axial divergence, it is convenient to use a reference sample, or in case that the substrate material is known and reproducible, the best option is to use the same substrate as an internal reference. As with the texture analysis, it is important to remember that the  $2\theta/\omega$  scan only gives information of the out-of-plane lattice parameters. There are several methods for determining the in-plane lattice parameters, such as, residual stress analysis (using a  $\psi$  tilt), RSMs, and in-plane diffraction, but unfortunately, these techniques are out of the scope of this article.

#### *Peak shape: Grain size and microstrain*

In  $2\theta/\omega$  scans the  $hkl$  peaks show a particular broadening. There is a minimum broadening related to the primary beam divergence which is related to the chosen optics, and further broadening due to the emission profile. When no monochromator is used, peak broadening is mostly dictated by the convolution of  $K\sqrt{1}$  and  $K\sqrt{2}$  contributions to each peak. This is increasing proportional to  $\sin(\omega)$ . Even if  $K\sqrt{1}$  and  $K\sqrt{2}$  contributions can be deconvoluted, their individual widths progressively increase with  $\sin(\omega)$ . Together, broadening due to the optics and emission profile is known as *instrumental* broadening. This is best checked by comparing to peaks from a single crystal substrate or standard wafer at a similar  $2\theta$  angle (see inset of **Fig. 7b**). Often the substrate peaks in the  $2\theta/\omega$  scan offer an easy and useful method of measuring the instrumental broadening. Other than instrumental broadening, information on the microstructure can be extracted from the shape of the  $hkl$  peaks, which is sometimes referred to as *line profile analysis*.

<sup>22</sup> In films with a complex microstructure consisting of a collection of domains with different orientation (twin domains, different orientation variants, i.e. a/c-oriented domains of tetragonal structure) or different shear distortions (monoclinic and triclinic structures) the accurate cell parameter determination requires first a model for the domain tilt. Once these tilts are taken into account the cell parameters can be extracted.

A primary source of peak broadening is related to the crystal domain size. In fine grained materials (nanometric or submicron size) the relationship between peak width and the average grain size is given by the Scherrer equation:

$$\beta_{\tau} = \frac{K\lambda}{\tau \cos \theta_{hkl}} \quad (2)$$

Where  $\lambda$  is the X-ray wavelength;  $\tau$  is the crystal domain size, and  $\theta$  is half the Bragg angle  $2\theta$ .  $\beta_{\tau}$  is the peak broadening (after subtracting the instrumental broadening)<sup>23</sup> corresponding to the FWHM (in radians!) of a particular  $hkl$  reflection.  $K$  is a geometrical constant, normally taken as 0.9 (0.94 for spherical grain with cubic crystal symmetry)<sup>24</sup>.<sup>[5]</sup> In epitaxial films the crystal coherence can extend to the whole film thickness, and therefore the peak broadening reflects the film thickness, the thinner the films the broader the corresponding peaks.

However, in thin films one has to be aware that there are other sources of peak broadening which could be larger than that of crystal domain size. As mentioned before, thin film materials are prone to retain some lattice strain which affects their average structure, shifting the peak positions, often named *macrostrain*. In those cases, it is also possible that, at a microscopic level, there is a distribution of strain, for example, within grains from the boundary to the core. This is called *microstrain*, and also affects the peak broadening. The relationship between the peak width and microstrain is given by the Wilson equation.

$$\beta_{\epsilon} = 4 \epsilon \tan \theta_{hkl} \quad (3)$$

where  $\epsilon$  is the microstrain, and  $\beta_{\epsilon}$  is the FWHM of the peak after subtraction of the instrumental broadening.<sup>25</sup> Microstrain is caused by different type of defects (local defects, dislocations, antiphase boundaries) which induce a inhomogeneous distribution of cell distortions, but could be also caused by some local inhomogeneity in composition or in strain relaxation.<sup>26</sup>

Because both grain size and microstrain cause peak broadening, it is usually necessary to distinguish between the two when characterising a film. Fortunately, both affect the peak shape in different ways. The broadening due to grain size leads to a Lorentz profile, while microstrain leads to a Gaussian profile. It is, therefore, recommended to fit  $hkl$  peaks with a *pseudo-Voigt* function, which is a linear combination of Lorentzian and Gaussian components. From the parameters of the fit, the  $\beta_{\tau}$  and  $\beta_{\epsilon}$  widths can be extracted. Alternatively, it can be seen from Eq. 2 and Eq. 3 that both contributions have a different angular dependence, so

<sup>23</sup>  $\beta_{\tau} = (B - b)$  where  $B$  is the FWHM of the film peak and  $b$  the FWHM of a perfect crystal due to instrumental broadening.

<sup>24</sup> If  $\beta_{\tau}$  refers to the integral breadth of the peak rather than the FWHM, then for spherical grain with cubic crystal symmetry  $K=0.89$ .

<sup>25</sup>  $\beta_{\epsilon} = (B^2 - b^2)^{1/2}$  where  $B$  is the FWHM of the film peak and  $b$  the FWHM of a perfect crystal due to instrumental broadening.

<sup>26</sup> As previously discussed, cell parameters may vary as a function of slight deviations in composition. It is often observed in electroceramics that chemical composition may vary at the microscale, i.e. from the core to the boundary of a single grain, or even at nanoscale, i.e. typical in morphotropic phase boundaries of ferroelectric materials, or martensitic structures. This may represent a source of "chemical" micro-strain difficult to distinguish from any other source.

having access to a collection of peak broadening of different  $hkl$  reflections in a sufficiently large  $2\theta$  range could help to separate both contributions. One simple method to evaluate crystal domain size and microstrain is the Williamson-Hall plot method. Eq. 2 and Eq. 3 can be combined ( $\beta = \beta_{\tau} + \beta_{\epsilon}$ ) to give:

$$\beta \cos \theta_{hkl} = \frac{K\lambda}{\tau} + 4\epsilon \sin \theta_{hkl} \quad (4)$$

The first term is  $\theta$  angle independent, while the second one depends only on  $\sin \theta_{hkl}$ . Therefore, in a  $\beta \cos \theta$  vs.  $\sin \theta$  representation, as shown in **Fig. 15**, the data should follow a linear dependence. The slope, either positive or negative, is directly  $4\epsilon$ , and the coordinate at origin is  $K\lambda/\tau$ . By plotting the data in this way, it is possible to determine if the peak shape is dominated by grain-size broadening, microstrain broadening, or a combination of the two, as well as extract values for each.

**Fig. 15** Williamson-Hall plot for a polycrystalline film where the peak broadening is dominated by either the grain-size, microstrain, or a combination of the two

### *Analysing rocking curves*

Rocking curves are especially useful when comparing between a set of films, where perhaps, the deposition parameters have been varied to optimise growth conditions. The width of the rocking curves will depend on the epitaxial quality (i.e. how well aligned the  $hkl$  planes of the film are), the dislocation or defect density, and the curvature of the film. When comparing between rocking curves, it is often useful to plot them as a function of the normalised intensity vs.  $\Delta\omega$ , where  $\Delta\omega=0^\circ$  is the centroid position. The peaks should be fit by a Gaussian curve with the FWHM giving an indication of the texture or epitaxial quality, as shown schematically in **Fig. 10**. Table 2 gives an idea of the values for the FWHM one might expect for various films. Rocking curves should be taken from each distinct family of planes present in the  $2\theta/\omega$  scan, as differently oriented grains will often have different degrees of alignment with the substrate.

**Table 2** Rocking curve widths for different types of films

| Type of sample        | FWHM of rocking curve |
|-----------------------|-----------------------|
| Semiconductor epitaxy | $<0.1^\circ$          |
| Oxide epitaxy         | $0.1-2^\circ$         |
| Strongly textured     | $<3^\circ$            |

It is worth bearing in mind that instrumental factors such as defocusing and a changing beam footprint on the sample or may contribute to the broadening of the rocking curves. As with the  $2\theta/\omega$  scan, a good method to check the resolution of the instrument is to perform a rocking curve on a high-quality single crystal at a similar  $2\theta$  angle as the film peak being analysed. This could be the substrate of the film itself or a standard sample such as a Si wafer.

### *Analysing pole figures and azimuth scans*

Regarding the presentation of pole figures, there are several different possibilities for projecting the hemisphere shown in **Fig. 11** onto a circular plane, where the radius can either be  $\sin\psi$  (perpendicular projection),  $\tan\frac{\psi}{2}$  (stereographic projection),  $\sqrt{2}\sin\frac{\psi}{2}$  (equal area projection), or  $\psi$  (constant  $\psi$  projection). The choice of projection will just affect the scaling and can be selected depending on the tilt angles of the reflections which are being visualised in the figure. The azimuth,  $\phi$ , should be oriented such that  $\phi = 0$  lies along a defined direction, such as a one of the planes of the substrate.

At a basic level, the analysis of pole figures and azimuth scans are primarily based on identifying either the presence or absence of certain peaks to build up an orientation relationship. Usually the out-of-plane orientation needs to be known, and so a  $2\theta/\omega$  scan should be performed prior to a pole figure or  $\phi$  scan. Peaks should appear at a  $\psi$  angle related to the interplanar angle (Table S2 in the supplementary information) between the out-of-plane orientation and the Bragg angle the diffractometer is set to. The number of peaks seen at a given  $\psi$ , in either the pole figure or  $\phi$  scan will determine the number of distinct in-plane orientations. For cubic materials it may be possible to visualise the system and work out the orientation from the interplanar angles. For non-cubic systems it is often necessary to use software to generate a stereographic projection. A good option is WinWULFF which is available online and free to download.[6]

By measuring multiple pole figures from a sample, a full understanding of the texture of a film can be developed. This can include quantifying the volume percentage of the film with a particular texture component, which may be defined by all the crystallites within a certain mis-orientation of a particular orientation with respect to a substrate axis. Multiple texture components can also be explored to compare the percentage by volume of one against another and compared with a random distribution of grains. A more comprehensive analysis of pole figures is possible using the crystallite Orientation Distribution Function (ODF). The ODF provides a full quantitative description of the texture as a function of volume percentage in the film.[7] A free software tool box for MATLAB called MTEX is available for analysing and modelling crystallographic textures from data such as pole figures.[8]

### **Summary and outlook**

XRD is an invaluable technique for thin film research and engineering, providing information on the crystal structure, texture, microstructure, stress/strain, composition, and thickness. It can, however, be a challenging or even overwhelming topic when starting out due to the range of XRD methods available, the requirements for aligning one's sample, and the interpretation of the resultant

data. In this tutorial, we have provided the information needed to bring the new experimentalist/engineer up to speed on XRD techniques for electroceramic thin films, in a way that is hopefully accessible and built on a solid foundation.

We have described five of the commonly used measurements: Symmetric  $2\theta/\omega$  scans, grazing-incidence scans, rocking curves, pole figures, and  $\phi$ -scans, which, together provide a rich variety of information and often form the basis of thin film analysis. By including a description of the features of the instrument, as well as guidelines on sample alignment, choosing scan conditions, and analysing data, it is our hope that inexperienced researchers may approach their first measurements with a sense of purpose of what they wish to achieve and have an understanding on how to go about it.

Building on this foundation, the aspiring thin film experimentalist/engineer should find the existing literature and resources more accessible, and begin to explore more advanced XRD techniques, such as:

- X-ray reflectivity (XRR) – An especially useful technique for determining the thickness, roughness, and density of films (not strictly diffraction). Unfortunately, a detailed explanation was out of the scope of this article, but for the interested user a good starting point is Ref. [9]
- Reciprocal space mapping (RSM) – Used for determining changes in the lattice parameters for both out-of-plane and in-plane axes due to stress/strain or compositional.
- In-plane XRD (requires a five-axis goniometer) – Measuring the Bragg reflections of planes perpendicular to the surface of the film to extract in-plane lattice parameters.
- Residual stress analysis – Measuring changes in the position of a Bragg reflection at different orientation of the sample relative to the X-ray beam to determine the stress state of films.
- Orientation distribution functions (ODFs) – Describes the density of orientations for an ensemble of grains in a polycrystalline material. Can be based on a series of XRD pole figure measurements, electron-backscattered diffraction (EBSD), or neutron diffraction.
- Whole pattern fitting – Useful for randomly oriented polycrystalline films or powder patterns, using Le Bail or Pawley fits to determine the unit cell lattice parameters or Rietveld refinement to determine the crystal structure. Crystallite size and microstrain analysis can be included in this analysis.
- Micro-XRD ( $\mu$ XRD) – Allows XRD analysis on very small areas or sample mapping.
- Non-ambient XRD – Performing *in situ* or *operando* XRD experiments in controlled environments (high/low temperatures, gas atmospheres, under electric fields, mechanical load).
- XRD at synchrotron facilities – Synchrotrons can provide high-intensity, highly monochromatic, and spatially defined X-ray beams which are useful for ultrathin films ( $<10\text{nm}$ ), spatially resolved XRD, dynamic studies (such as non-ambient XRD as mentioned above), films with light elements that have weakly scattering cross-sections, or for studying very weak reflections coming from, for example, subtle structure distortions, point/planar defects, crystal domain twinning, or diffuse scattering.



## Further reading and resources

### *Textbooks and book chapters*

- Elements of X-Ray Diffraction by B.D. Cullity, S.R. Stock - Latest version of a classic textbook on X-ray diffraction.[10]
- Thin Film Analysis by X-ray Scattering by M. Bikholtz - Excellent and comprehensive textbook of thin film analysis using XRD and XRR.[7]
- High-Resolution X-Ray Scattering: From Thin Films to Lateral Nanostructures by U. Pietsch, V. Holy, and T. Baumbach[11]
- High Resolution X-Ray Diffractometry And Topography by D.K. Bowen and B.K. Tanner[12]
- Chapter on In Situ High-Temperature X-ray Diffraction of Thin Films: Chemical Expansion and Kinetics by J. Santiso, R. Moreno in Electro-Chemo-Mechanics of Solids.[13]

### *Online resources*

- Collaborative Computational Project Number 14 (CCP14) - Collection of freely available crystallographic software and tutorials for students and academia [14]
- International Union of Crystallography (IUCr) website - Website with links to journals, tutorials, software, and databases[15]
- Massachusetts Institute of Technology X-ray Diffraction Shared Experimental Facility webpage - Excellent resource with tutorials, standard operating procedures for certain instruments, and curated lists of literature, tutorials, online resource, and software[16]
- Powder Diffraction on the WEB - Open access online course on powder diffraction developed by the former Industrial Materials Group, Birkbeck College, University of London[17]
- Rigaku Journal - Journal produced by the diffractometer manufacturer Rigaku, publishing application notes and technical articles on methods including XRD[18]
- Malvern Panalytical Knowledge Center - Online resource of technical notes and application notes on various methods and applications by the diffractometer manufacturer Malvern Panalytical[19]
- Bruker webinars - Online webinars organised by the diffractometer manufacturer Bruker on techniques[20]

### *Crystallography databases*

- Crystallography Open Database (COD) - Free online database of crystal structures[21]
- Inorganic Crystal Structure Database (ICSD) - Commercial database produced by FIZ Karlsruhe[22]
- Powder Diffraction File (PDF) - Commercial database by the International Centre for Diffraction Data (ICDD)[23]

### *Software*

- PowDLL Converter - Free software for converting between various output files from different diffractometer software[24]

- JCrystalSoft - Collection of free crystallography software including WinWULFF, which is excellent for generating stereographic projections[25]
- MTEX Toolbox - Free toolbox for MATLAB for analysing and modelling texture from pole figure data. Also can be used for EBDS analysis.[26]

## Acknowledgements

We gratefully acknowledge D. Klotz and H.L Tuller for critically reading the manuscript. GFH acknowledges support from The Japanese Science and Technology Agency (JST) through its Center of Innovation Program (COI Program, grant number: JPMJCE1318) and the International Institute for Carbon-Neutral Energy Research (WPI-I2CNER), supported by MEXT, Japan. ICN2 is funded by the CERCA programme/Generalitat de Catalunya and by the Severo Ochoa programme of the Spanish Ministry of Economy, Industry and Competitiveness (MINECO, grant no. SEV-2017-0706). The datasets generated during and analysed during the current work are available from the corresponding author on reasonable request.

## References

- [1] G. Hölzer, M. Fritsch, M. Deutsch, J. Härtwig, and E. Förster, " $K\alpha_{1,2}$  and  $K\beta_{1,3}$  x-ray emission lines of the 3d transition metals," *Phys. Rev. A - At. Mol. Opt. Phys.*, vol. 56, no. 6, pp. 4554–4568, 1997.
- [2] T. Mitsunaga, "X-ray thin-film measurement techniques II. Out-of-plane diffraction measurements," *Rigaku J.*, vol. 25, no. 1, pp. 7–12, 2009.
- [3] T. Konya, "X-ray thin-film measurement techniques III. High resolution X-ray diffractometry," *Rigaku J.*, vol. 25, no. 2, p. 1, 2009.
- [4] M. Ohring, *Materials Science of Thin Films*, 2nd Editio. Elsevier, 2002.
- [5] J. I. Langford and A. J. C. Wilson, "Scherrer after sixty years: A survey and some new results in the determination of crystallite size," *J. Appl. Crystallogr.*, vol. 11, no. 2, pp. 102–113, 1978.
- [6] S. Weber, "WinWulff 1.6, www.jcrystal.com." 2018.
- [7] M. Birkholz, *Thin Film Analysis by X-Ray Scattering*. Weinheim: WILEY-VCH Verlag GmbH & Co. KGaA, 2006.
- [8] F. Bachmann, R. Hielscher, and H. Schaeben, "Texture Analysis with MTEX - Free and Open Source Software Toolbox," *Solid State Phenom.*, vol. 160, pp. 63–68, 2010.
- [9] Yasaka Miho, "X-ray thin-film measurement techniques V. X-ray reflectivity measurement," vol. 26, no. 2, pp. 1–9, 2010.
- [10] B. D. Cullity and S. R. Stock, "Elements of X-ray Diffraction," *Prentice Hall, New Jercey*, p. 531, 2001.
- [11] U. Pietsch, V. Holy, and T. Baumbach, *High-Resolution X-Ray Scattering: From Thin Films to Lateral Nanostructures*. Springer-Verlag New York, 2004.
- [12] D. K. Bowen and B. . Tanner, *High Resolution X-Ray Diffractometry And*

- Topography*. London: CRC Press, 1998.
- [13] J. Santiso and R. Moreno, "In Situ High-Temperature X-ray Diffraction of Thin Films: Chemical Expansion and Kinetics," in *Electro-Chemo-Mechanics of Solids*, Springer, Cham, 2017, pp. 35-60.
- [14] "The CCP14 (Collaborative Computational Project No. 14) in Powder and Small Molecule Single Crystal Diffraction." [Online]. Available: [www.ccp14.ac.uk](http://www.ccp14.ac.uk).
- [15] "International Union of Crystallography." [Online]. Available: [www.iucr.org](http://www.iucr.org).
- [16] "Massachusetts Institute of Technology X-ray Diffraction Shared Experimental Facility." [Online]. Available: [prism.mit.edu/xray](http://prism.mit.edu/xray).
- [17] J. K. Cockcroft and P. Barnes, "Powder Diffraction on the WEB." [Online]. Available: [pd.chem.ucl.ac.uk/pd/welcome.htm](http://pd.chem.ucl.ac.uk/pd/welcome.htm).
- [18] "Rigaku Journal." [Online]. Available: [www.rigaku.com/downloads/rigaku-journal](http://www.rigaku.com/downloads/rigaku-journal).
- [19] "Malvern Panalytical Knowledge Center." [Online]. Available: [www.malvernpanalytical.com/en/learn/knowledge-center](http://www.malvernpanalytical.com/en/learn/knowledge-center).
- [20] "Bruker Webinars." [Online]. Available: [www.bruker.com/service/education-training/webinars.html](http://www.bruker.com/service/education-training/webinars.html).
- [21] "Crystallography Open Database (COD)." [Online]. Available: [www.crystallography.net/cod](http://www.crystallography.net/cod).
- [22] "Inorganic Crystal Structure Database (ICSD)." [Online]. Available: [icsd.products.fiz-karlsruhe.de](http://icsd.products.fiz-karlsruhe.de).
- [23] "Powder Diffraction File (PDF)." [Online]. Available: [www.icdd.com](http://www.icdd.com).
- [24] N. Kourkoumelis, "PowDLL, [users.uoi.gr/nkourkou/powdll](http://users.uoi.gr/nkourkou/powdll)." 2013.
- [25] S. Weber, "JCrystalSoft, [www.jcrystal.com](http://www.jcrystal.com)." 2019.
- [26] R. Hielscher *et al.*, "MTEX Toolbox, [mtex-toolbox.github.io](http://mtex-toolbox.github.io)." 2021.